Int. J. Electrochem. Sci., 11 **(2016)** 7125 – 7138, doi: 10.20964/2016.08.71

International Journal of ELECTROCHEMICAL SCIENCE
www.electrochemsci.org

Comparison of Corrosion Resistance and Corroded Surfaces of Welding Metal in Overlay-Welded Inconel 600 and Inconel 625 by Gas Metal Arc Welding

Eui-je Jung, Hae-woo Lee[*]

Department of Materials Science and Engineering, Dong-A University, Busan, Rep. of Korea
[*]E-mail: hwlee@dau.ac.kr

Received: 9 May 2016 / *Accepted:* 21 June 2016 / *Published:* 7 July 2016

Inconel is a Ni-based alloy with high strength and high corrosion resistance at high temperature. In this study, the corrosion resistance of overlay-welded Inconel 600 and Inconel 625 in carbon steel pipes was compared in various corrosion tests. The pitting resistance, intergranular corrosion resistance, and intergranular sensitization level of samples overlay-welded with gas metal arc welding (GMAW) under the same welding condition, through potentiodynamic polarization, potentiostatic polarization, and double-loop electrochemical potentiokinetic reactivation (DL-EPR) tests, and the corroded surfaces were observed through scanning electron microscopy coupled with energy-dispersive X-ray spectroscopy(SEM-EDS). Results of the potentiodynamic polarization test showed that Inconel 625 had slightly higher corrosion potential, pitting potential, and passive region than Inconel 600. The potentiostatic polarization test also showed that both the pitting resistance and intergranular corrosion resistance were higher in Inconel 625 than in Inconel 600 because Inconel 625 had a lower current. In the DL-EPR test, since sensitization occurred at the grain boundary in Inconel 600, its degree of sensitization (DOS) could be obtained; however, sensitization did not occur in Inconel 625, leaving its DOS undetermined.

Keywords: Inconel 625, Inconel 600, Overlay welding, Gas metal arc welding, Corroded surfaces

1. INTRODUCTION

Inconel, which is a Ni group alloy, is a material with super heat resistance, and the main alloying elements of Inconel 600 are Ni–Cr and those of Inconel 625 are Ni–Cr–Mo. Inconel 600 and Inconel 625 are both solid-solution-strengthened alloys, which have high strength at high temperatures and excellent corrosion resistance **[**1**]**. However, because Inconel alloys use expensive Ni as the main element, they are economically inefficient, so they are used as welding materials rather than main

materials, especially in heterojunctions or overlay welding. In general, the corrosion resistance of the overlay welding metal is higher than that of the heterojunction welding metal because the difference between thermal expansion coefficients of the heterojunction welding metal and base metal is larger than that between the overlay welding metal and base metal. The difference between the thermal expansion coefficients of the welding metal and base metal induces thermal fatigue cracking and stress corrosion cracking (SCC). Therefore, studies were also carried out recently on the expected improvement in corrosion resistance by adding an overlay welding metal on top of the heterojunction metal **[**2–6].

Inconel 600 has low SCC susceptibility for chloride, good machinability, and mechanical properties. Also, because its weldability is high compared to other materials with high corrosion resistance, and the resistance against intergranular corrosion and SCC is enhanced by post-welding heat treatment (PWHT), it is often used in pipes transporting nuclear energy, internal walls and machinery or equipment of a nuclear reactor, petrochemical equipment, and offshore plants. However, its pitting resistance is rather weak in high-temperature sea water, and the alloy is very susceptible to SCC in a sulfide-containing atmosphere. Moreover, it has the disadvantage of hydrogen embrittlement in the presence of H_2 at high temperatures [7–12]. Therefore, there have been recent efforts to replace Inconel 600, and many studies are being carried out to compare its strength and corrosion characteristics at high temperatures with those of other Ni alloys and high-corrosion-resistance materials **[**13–15**]**. On the other hand, Inconel 625 has high oxidation resistance because of its high Cr content and excellent resistance against SCC and intergranular corrosion. Also, because its mechanical strength is high at high temperatures, its use is gradually extended to structural materials of nuclear power plants and offshore plants **[**1**]**. As the usage range of Inconel 625 broadens, more and more studies are conducted on the improvement of the alloy's mechanical strength or anti-corrosion property by PWHT or grain refinement **[**16**]**. Depending on the heat-treatment temperature and duration selected for Inconel 625, many second phases and carbides are precipitated , mainly as a result of reactions with alloying elements such as Ni, Cr, Al, Ti, Nb, and C. Among them, the Laves phase and δ phase are compounds of Ni and Nb metals produced at 1123 K (850 °C) or higher, and they not only decrease toughness, fatigue strength, and creep strength, but also reduce the anti-corrosion property. Accordingly, studies were carried out to investigate the changes in microstructure and changes in mechanical and anti-corrosion properties caused by the precipitation of second phases and carbides according to the PWHT temperature and duration [17,18]. Unlike metals in common welding or heterojunctions, the microstructures of the overlay welding metal are all dendrites, which affects the strength and corrosion resistance, especially during heat treatment, because the laves phase is extracted between dendritic grain boundaries, thus decreasing the strength and corrosion resistance [19].

Inconel 600 and Inconel 625 are often used for overlay welding in nuclear power plants and offshore plants because of their high strength and high corrosion resistance. Since the corrosion resistance of materials in various oxidative atmospheres is especially important in nuclear power plants, it has been investigated in many studies [9,20]. However, these studies mostly compare high-alloy steels, which are different from Inconel alloys, or deposited metals at heterojunctions instead of overlay welding metals; no study has been conducted to compare the corrosion resistance of overlay-welded Inconel 600 and Inconel 625 in oxidation atmospheres. Therefore, in our study on the overlay

welding metals of Inconel 600 and Inconel 625, the pitting resistance, intergranular corrosion resistance, and degree of sensitization were compared through various corrosion tests; and each of their corrosion characteristics were compared by comparative analysis using a scanning electron microscope equipped with an energy-dispersive X-ray spectrometer (SEM–EDS).

2. EXPERIMENTAL METHOD

2.1. Fabrication of samples

In this study, overlay welding was performed by gas metal arc welding (GMAW). As filler metals, UNS N06082 (NiCr-3) and UNS N06625 (NiCr22Mo9Nb) were used for Inconel 600 and Inconel 625, respectively; ASTM A333 Grade 6 carbon steel was used as the base metal. The overlay thickness was 4 mm, and the base metal thickness was 21 mm. Fig. 1 shows a schematic diagram of the welding metal's shape and the test sample. To perform a metallurgical analysis, the welding conditions of the samples were kept uniform, and the values are specified in Table 1. Table 2 shows the composition of carbon steel, which is the base metal, and the composition of the welding materials and welding wires, Inconel 600 and Inconel 625. The composition of the welding metal was determined by taking the average of five measurements obtained by a spark emission spectrometer(Metal–Lab75/80J, GNR srl, Italy).

Table 1. Welding conditions of the alloy samples.

Welding rod	Welding current (A)	Welding voltage (V)	Welding rate (cpm)	Feed rate (cpm)
Inconel 600 Inconel 625	**193**	**14**	**19.6**	**105**

Table 2. Chemical composition of welding materials.

Type	Ni	Cr	Fe	Mo	Nb	Mn	C
Inconel 600 wire	71.9	20.32	1.04	–	2.44	3.09	0.02
Inconel 625 wire	63.8	22.24	3.7	8.67	3.36	0.03	0.01
Inconel 600 overlay bead	69.5 ± 0.5	18.1 ± 0.6	6.25 ± 0.16	0.02 ± 0.01	2.44 ± 0.05	2.85 ± 0.24	0.28 ± 0.03
Inconel 625 overlay bead	62.1 ± 1.2	20.9 ± 1.8	5.17 ± 0.2	8.27 ± 0.3	3.54 ± 0.3	0.07 ± 0.01	0.18 ± 0.06
A333 Gr. 6	0.05 ± 0.01	0.08 ± 0.01	98.4 ± 0.1	–	–	0.95 ± 0.01	0.18 ± 0.01

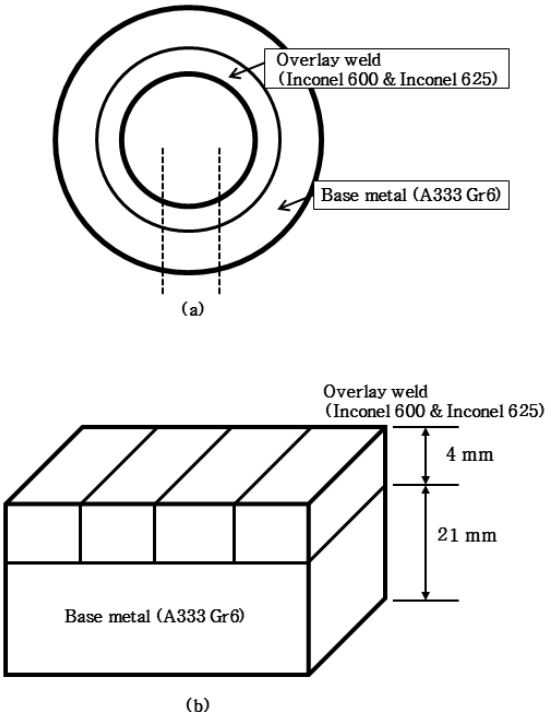

Figure 1. (a) Cross-sectional schematic diagram of Inconel 625 and Inconel 600 overlay-welded pipe. (b) Schematic diagram of the test sample.

2.2. Corrosion test and observation of corroded surface

2.2.1. Pitting test

To compare the pitting resistance of each sample, an electro-chemical test was conducted along with the potentiodynamic polarization test using a potentiostat/galvanostat (VersaSTAT3, Princeton Applied Research, USA). The test samples were prepared by ultrasonic cleaning using 75% ethanol after mechanical polishing with 2000-grit SiC paper [21]. To examine the corrosion resistance of the Inconel alloys, polarization tests were performed in a mixed solution consisting 1 M H_2SO_4 and 0.5 M NaCl. Before conducting the polarization tests, an open-circuit potential (OCP) was applied for 20 min to form a stable passive film on the samples' surfaces [21]. The corrosion cell used in the corrosion experiment was a K0235 flat cell, and the test area was set at 1 cm^2. The reference electrode was Ag–AgCl/KCl (sat'd), the counter electrode was platinum foil, and the working electrode was the test sample. The polarization test was conducted at room temperature (298 K or 25 °C); the electric potential range was set from –0.5 mV (initial potential) to 1.5 mV (final potential); and the scan rate was 0.5 mV/s.

2.2.2. Intergranular corrosion test

To examine the intergranular corrosion resistance and sensitization, two electro-chemical tests—the potentiostatic polarization test and the double-loop electrochemical potentiokinetic

reactivation (DL-EPR) test—were carried out. The VersaSTAT3 potentiostat/galvanostat used in the potentiodynamic polarization test was used, and OCP was performed for 20 min to form a stable passive film on the sample surfaces prior to conducting the tests.

The potentiostatic test was carried out at room temperature in a solution of 2 M H_2SO_4 and 0.5 M NaCl. Two kinds of test were conducted by changing the electric potential: considering that the pitting potential values of the two samples were about 1–1.4 V through OCP, the electric potential was set at 1 and 1.5 V, which are higher than the pitting potential. The test period was 1 h.

The DL-EPR test was carried out according to the International Standard ISO 12732 in a mixed solution consisting 2 M H_2SO_4, 2 M HCl, and 0.5 M NaCl [22]. For the potential range, the initial potential was set at –1 mV, the vertex potential at 2 mV, and the final potential at –1 mV according to the pitting potential values measured in OCP; the scan rate was set at 0.5 mV/s. The values of intergranular corrosion resistance were compared by measuring the degree of sensitization (DOS) from the ratio $I_r/I_a \times 100$ of the maximum anode current density (I_a) in an anodic loop, which is when the potential is increasing in the DL-EPR test, and the maximum anode current density (I_r) in a reactivation loop, which is when the potential is decreasing.

After each corrosion resistance test, the corrosion form and chemical composition were observed by SEM–EDS(JSM–6700f, jeol, Japan) at an acceleration voltage of 20 kV.

3. RESULTS AND DISCUSSION

3.1. Pitting test results

Fig. 2 shows polarization curves obtained from the potentiodynamic polarization tests carried out in the mixed solution of 1 M H_2SO_4 and 0.5 M NaCl for the welding metals Inconel 600 and Inconel 625. Overall, the polarization curve of Inconel 625 has higher potential values than those of Inconel 600. For more accurate and easier analysis, the values of corrosion potential (E_{corr}), pitting potential (E_{pit}), passive region (ΔE), and corrosion current (I_{corr}) for the two welding metals are shown in Table 3. The E_{corr} value of Inconel 625 was –58.8 $mV_{Ag/AgCl}$, which is larger than E_{corr} = –245.7 $mV_{Ag/AgCl}$ of Inconel 600; the E_{pit} value of 1306 $mV_{Ag/AgCl}$ for Inconel 625 is higher than E_{pit} = 1011 $mV_{Ag/AgCl}$ of Inconel 600. According to Xu et al. [23], the corrosion resistance of materials can be compared with the width of the passive region (ΔE), which is a value obtained by subtracting the corrosion potential (E_{corr}) from the pitting potential (E_{pit}), i.e., $\Delta E = E_{pit} - E_{corr}$. In other words, as the width of the passive region increases in a potentiodynamic polarization graph, the value of ΔE increases, resulting in a more stable passive film [23]. As shown in Fig. 2, the passive region is marginally wider in the polarization curve of Inconel 625 than that of Inconel 600, and in Table 3, it can be confirmed that ΔE of Inconel 625 was about 100 mV higher. Furthermore, the size of the corrosion current density (I_{corr}) is an indicator of the corrosion resistance. As the corrosion current density becomes smaller, it signifies that a sample is becoming more stable, and because a stabilized passive state is not easily broken, the force resisting corrosion is large [23]. The corrosion current densities (I_{corr}) shown in Table 3 were obtained by extrapolation using the Tafel equation. It can be

confirmed that the current density of Inconel 625 was about 20 μA/cm^2 lower than that of Inconel 600. Because a larger amount of corrosion occurred in Inconel 600 than Inconel 625, a higher current density was obtained. According to a study by Hayes et al. [24], as the amount of added Cr increases in a Ni-based alloy, the pitting resistance improves because E_{corr} and E_{pit} increase; when pitting corrosion proceeds, a passive film is stabilized because of the addition of Mo and thus, intergranular corrosion resistance tends to increase. The chemical composition of the filler metal used in our experiment was 22.24 wt.% chromium and 8.27 wt.% molybdenum for Inconel 625, which is 4 wt.% higher in Cr and 8 wt.% higher in Mo than the composition of Inconel 600. Therefore, according to the study of Hayes et al. [24], it is thought that owing to the effect of Cr addition, the corrosion potential and breakdown potential increase, and due to the effect of Mo, a more stable film is formed, resulting in higher pitting resistance for Inconel 625 than Inconel 600. When the pitting resistance equivalent number (PREN) of Inconel 600 and Inconel 625 were obtained with a quantitative method, it was approximately 21 for Inconel 600, which is only half of the value of 40 for Inconel 625. In other words, the pitting resistance of Inconel 625 must be much better. However, the result of potentiodynamic polarization test in the solution of 1 M sulfuric acid and 0.5 M NaCl showed that Inconel 625 exhibited better pitting resistance, but it was not much different from the expected value. The value of PREN for a Ni–Cr–Mo alloy is calculated as follows:

$$PREN = wt.\%Cr + 1.5(wt.\%Mo + wt.\%W + wt.\%Nb) \quad (1)$$

Table 3. Values of anti-corrosion properties obtained via potentiodynamic polarization tests of Inconel 600 and Inconel 625.

Sample	E_{corr} ($mV_{Ag/AgCl}$)	E_{pit} ($mV_{Ag/AgCl}$)	ΔE (mV)	I_{corr} (μA/cm^2)
Inconel 600	–245.7	1011	1256.7	46.6
Inconel 625	–58.8	1306	1364.8	26.4

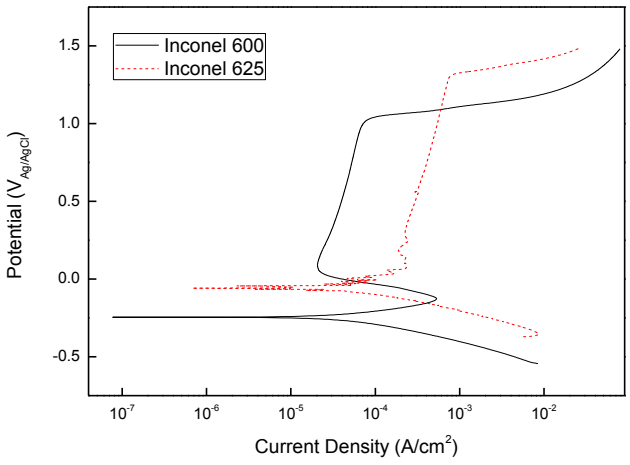

Figure 2. Comparison of potentiodynamic polarization curves of Inconel 600 and Inconel 625 in a solution of 1 M H_2SO_4 and 0.5 M NaCl at 25 °C.

3.2. Intergranular corrosion test results

Based on the results of the conducting potentiostatic polarization tests at 1 and 1.5 V to find the intergranular corrosion resistance of each sample, the graphs in Fig. 3 and residual current of each sample in Table 4 were obtained. At 1 V, the curve shapes of two samples had similar patterns, as shown in Fig. 3(a), but not much difference can be seen in the residual current values in Table 4. Nevertheless, Inconel 625 had a lower residual current than Inconel 600. As the residual current became smaller, a more stable and firmer passive region was obtained. As shown in Fig. 3(b), since the residual current value of Inconel 625 at 1.5 V was very low, it had a stable passive region. Furthermore, after a rapid decrease in the current, there was a section where the decrease became narrower with time and the passive film was stabilized. In the case of Inconel 625, the current value decreased rapidly and stabilized faster (less than 30 min) than that of Inconel 600. Therefore, the passive region of Inconel 625 was more stable and firmer than that of Inconel 600. In a study by Grosseau-Poussard et al., the potentiostatic polarization curves of pure Ni and Ni w with added Cr were compared [25]. The Cr-added sample had a noticeably lower current than the pure Ni sample. Accordingly, it is considered that when Cr is added to a Ni-based alloy in a potentiostatic polarization test, faster stabilization is obtained with a lower current value, and the intergranular corrosion resistance increases. Therefore, since the amount of Cr in the chemical composition of our Inconel 625 sample was about 4% larger than that in the chemical composition of our Inconel 600 sample, it had a marginally smaller current, and it is thought that the resistance for intergranular corrosion was better.

Table 4. Residual current in potentiostatic polarization tests of Inconel 600 and Inconel 625.

	Residual current	
	1 V	**1.5 V**
Inconel 600	6.08×10^{-4} mA	8.795 mA
Inconel 625	0.12×10^{-4} mA	0.002 mA

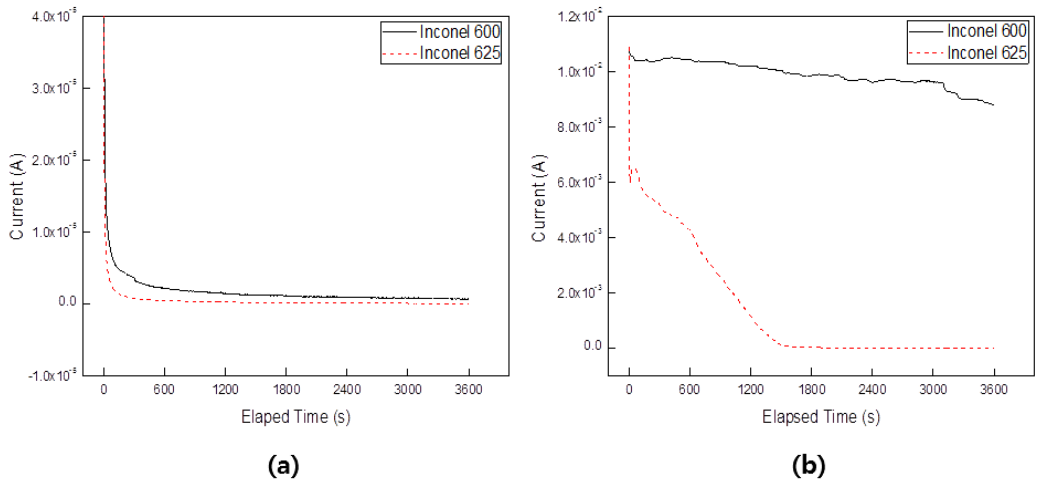

Figure 3. Potentiostatic polarization results for Inconel 600 and Inconel 625 at potentials of (a) 1 V and (b) 1.5 V.

Fig. 4 shows SEM images of the microstructure on the surface of Inconel 600 and Inconel 625 before the corrosion test. The polished samples were etched by immersion for 20 s in aqua regia, consisting of 30 mL of HCl and 10 mL of HNO_3. Fig. 5 shows SEM images of the observed corroded surfaces of the Inconel 600 and Inconel 625 samples after the potentiostatic polarization tests were conducted at 1.5 V, which is higher than the pitting potential. Both Figs. 4 and 5 show that both samples were composed of dendritic microstructures. Panels (a) and (b) of both figures show the surface of Inconel 600 at 500× and 1,000× magnification, respectively, and panels (c) and (d) of both figures show the surface of Inconel 625 observed at 500× and 1,000× magnification, respectively. In Figs. 4 and 5, the prominent bright regions correspond to the subgrain boundaries and the dark regions correspond to the columnar dendrite cores [17]. The subgrain boundaries appeared bright because of the presence of Nb carbide and oxide [1]. In the case of Inconel 600 in Fig. 5, the valley-like features show that corrosion proceeded in a wide surrounding region of the grain boundary, in contrast to Inconel 600 in Fig. 4. Because corrosion occurred at the grain boundary, the shape of the grain boundary can be clearly seen. Around the grain boundary where the corrosion occurred, a small amount of the second phase NbC precipitated. Since the pit became deeper in the direction from the transgranular region to the grain boundary, it was determined that the corrosion started from the grain boundary and progressed to the transgranular region. On the other hand, Inconel 625 exhibited a clear difference from Inconel 600: with the exception of oxides that were formed in a bright color at the subgrain boundaries, neither intergranular corrosion nor overall corrosion occurred. Because the grain boundary was not corroded, the location of the grain boundaries could be estimated only from the arrangement of the subgrain boundaries, which could not be clearly distinguished.

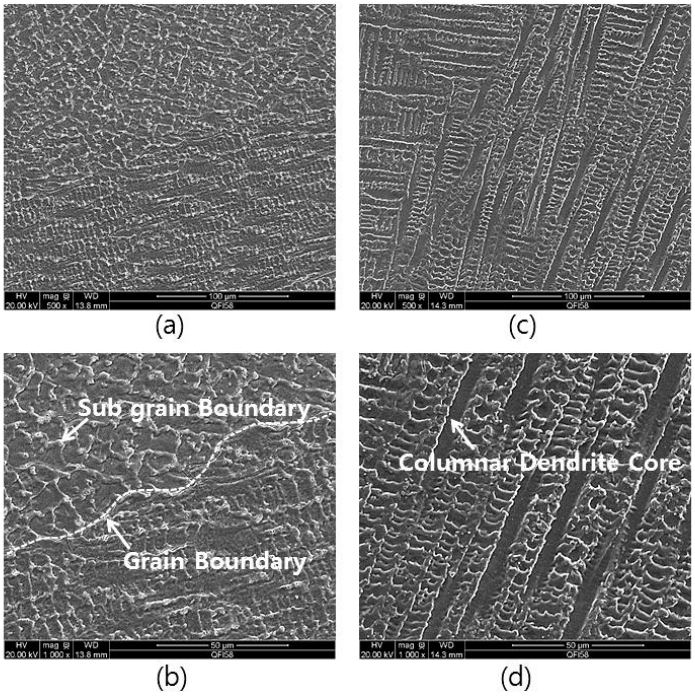

Figure 4. SEM images of the surface of etched samples before the corrosion test: Inconel 600 at (a) 500× magnification and (b) 1000× magnification; Inconel 625 at (c) 500× magnification and (d) 1000× magnification.

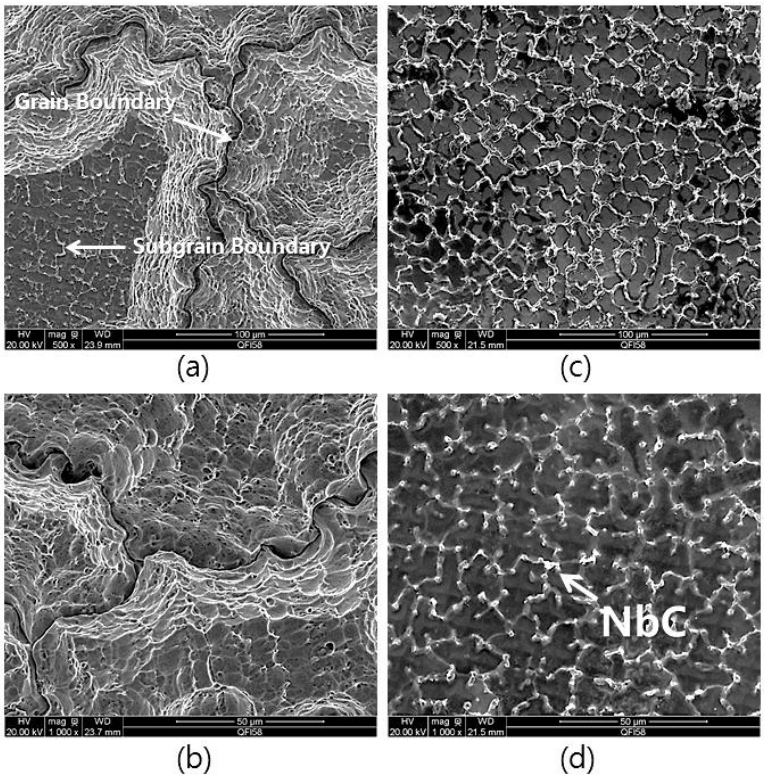

Figure 5. SEM images of the surface of samples after the potentiostatic polarization test at 1.5 V potential for Inconel 600 at (a) 500× magnification and (b) 1,000× magnification and for Inconel 625 at (c) 500× magnification, and (d) 1,000× magnification.

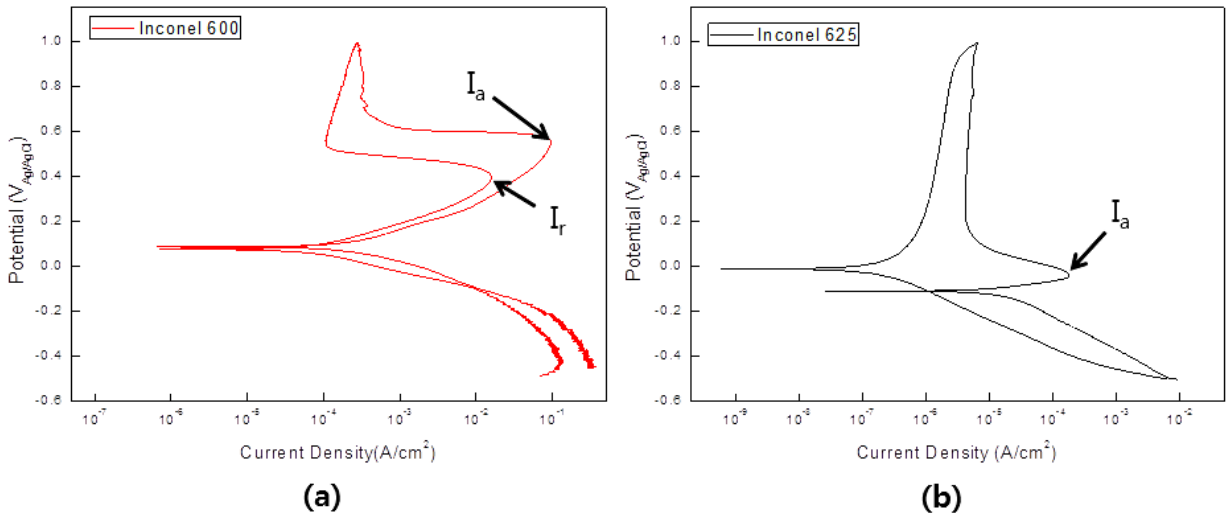

Figure 6. Graphs of cyclic polarization test results of (a) Inconel 600 and (b) Inconel 625.

The DL-EPR test results are shown in Fig. 6: Fig. 6(a) shows a graph of the cyclic polarization test results of the Inconel 600 sample in a solution of 2 M H_2SO_4 and 2 M HCl + 0.5 M NaCl; Fig. 6(b) shows a graph of the test results of Inconel 625 under the same conditions. The test values are summarized in Table 5. In the case of Inconel 600, the maximum anode current density I_a at the anodic loop was 132.79 mA, and the maximum anode current density I_r at the reactivation loop was 1.296

mA; and when DOS was obtained with these values, the ratio I_r/I_a was about 0.01. According to ISO 12732 [22], this value is within the range of fine sensitization. On the other hand, the value of I_a for Inconel 625 was 36.82 μA, but the value of I_r could not be obtained. Hayes et al. reported that Mo does not affect the pitting potential value, but it plays a role in delaying the intergranular corrosion by stabilizing the passive film [24]. Therefore, although the passive film was destroyed owing to the progression of corrosion, it is thought that because the corrosion rate was very slow because of the large amount of Mo, the value of I_r could not be obtained.

Table 5. DL-EPR test results of Inconel 600 and Inconel 625.

Sample	I_a	I_r	I_r/I_a
Inconel 600	132.79 mA	1.296 mA	0.01
Inconel 625	36.82 μA	–	–

Fig. 7 shows SEM images of the corroded surfaces of Inconel 600 and Inconel 625 samples after the DL-EPR test. The region shown in bright color in Fig. 7 corresponds to the interdendritic subgrain boundary shown in Fig. 4. More Nb and Mo existed in this region than in the surrounding area, and this was where Nb carbides were usually precipitated [17,28]. In contrast to Inconel 600, shown in Fig. 4(a) and (b), it was confirmed that much corrosion occurred at the subgrain boundaries in Inconel 600, shown in Fig. 7(a) and (b), and it was observed that Nb carbides were precipitated between the subgrain boundaries. On the other hand, as shown in Fig. 7(c) and (d), oxides were observed only at the subgrain boundaries of Inconel 625, and no cracking due to corrosion was observed. Furthermore, it can be confirmed that the surroundings of the grain boundaries were slightly corroded.

Fig. 8 shows the chemical composition of elements in the grain boundaries of the Inconel 600 sample, which was observed under 10,000× magnification through energy-dispersive X-ray spectroscopy (EDS). In the transgranular region, the concentrations of major elements such as Ni and Cr were similar to the composition of the sample analyzed using the spectrometer, except that C was 1.07 wt.%. However, the Nb content was measured to be about six times higher at the grain boundary than the concentration in the surrounding, and the concentrations of Ni and Cr were about 1/3 and 1/2 of those in the transgranular region. In addition, the concentration of C was 7.59 wt.%, which is very high because during overlay welding, the base metal's carbon spread to the welding metal and became diluted [19, 26]. As shown in Table 2, the concentration of the welding metal's carbon in both Inconel 600 and Inconel 625 were higher than the welding wires' carbon, which further confirms that the carbon became diluted. To see the distribution of elements around the grain boundary, images from the SEM–EDS chemical composition mapping analysis are shown in Fig. 9. A dark region in the figure means that the amount of an element is low, and the region where color is vivid means that the amount of an element is large compared to that in the surroundings. The dark intergranular region in Fig. 9(c)

means that a Cr-deficient region was formed. As shown in Fig. 9(d), the amount of Ni was also small around the grain boundary and the region appeared dark. In contrast, as shown in Fig. 9(b), since a large amount of oxygen existed at the grain boundary, corrosion must have occurred [27,28]. This can be explained by the dilution of carbon in overlay welding. The C that spread from the base metal and became diluted met Cr and formed Cr carbide at the grain boundary; accordingly, because the amount of Cr was low around the grain boundary, a Cr-deficient region was formed around the grain boundary. As a result, the reaction of Ni with O became easier and corrosion first occurred at the grain boundary region as the passive layer of Cr oxidation decreased [19,26]. It appears that the Inconel 600 sample was more sensitive to intergranular corrosion than the Inconel 625 sample because the amounts of Cr and Mo amounts were lower in Inconel 600. According to a study by Ren et al., a large difference can be created in the corrosion resistance even with a difference of about 2–3 wt.% in the Cr content [27]. Therefore, it is thought that intergranular corrosion could occur easier on the Inconel 600 sample, where the Cr content was about 4 wt.% smaller because of the presence of C, which has a high dilution rate in overlay welding. In contrast, owing to the effect of Mo added in large quantity on the Inconel 625 sample, the passive film was more stabilized more and was not easily destroyed; and even if destroyed, the rate of corrosion was delayed [24]. Therefore, we conclude that Inconel 600 is more sensitive to intergranular corrosion than Inconel 625.

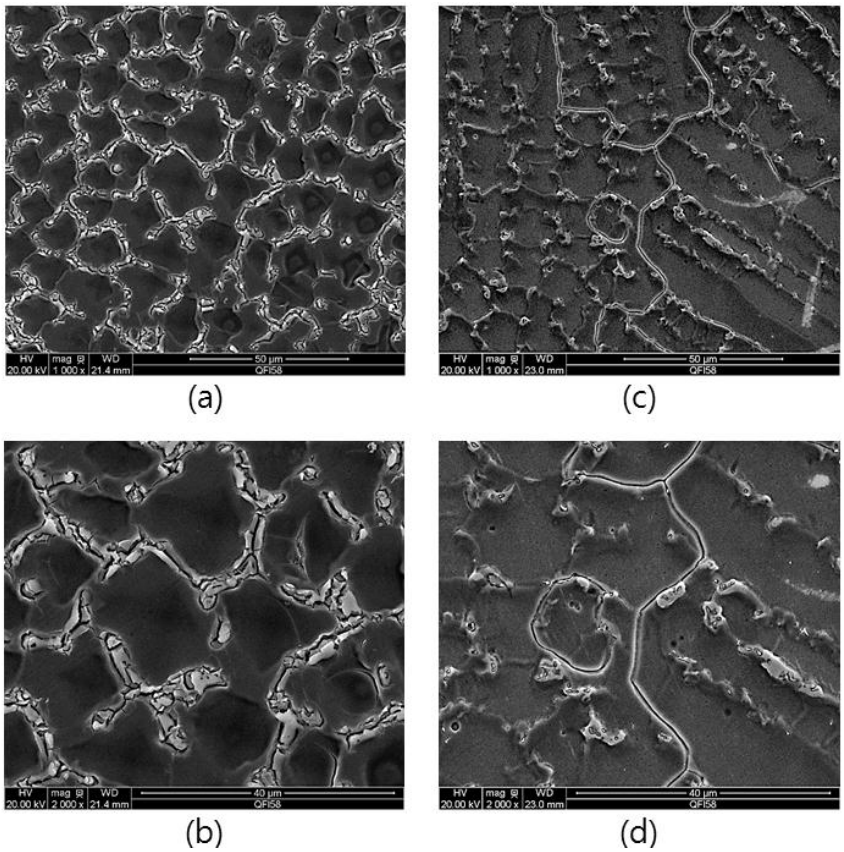

Figure 7. SEM images after the DL-EPR test: corroded surface of the Inconel 600 sample at 1,000× magnification and (b) 2,000× magnification; corroded surface of the Inconel 625 sample at (c) 1,000× magnification and (d) 2,000× magnification.

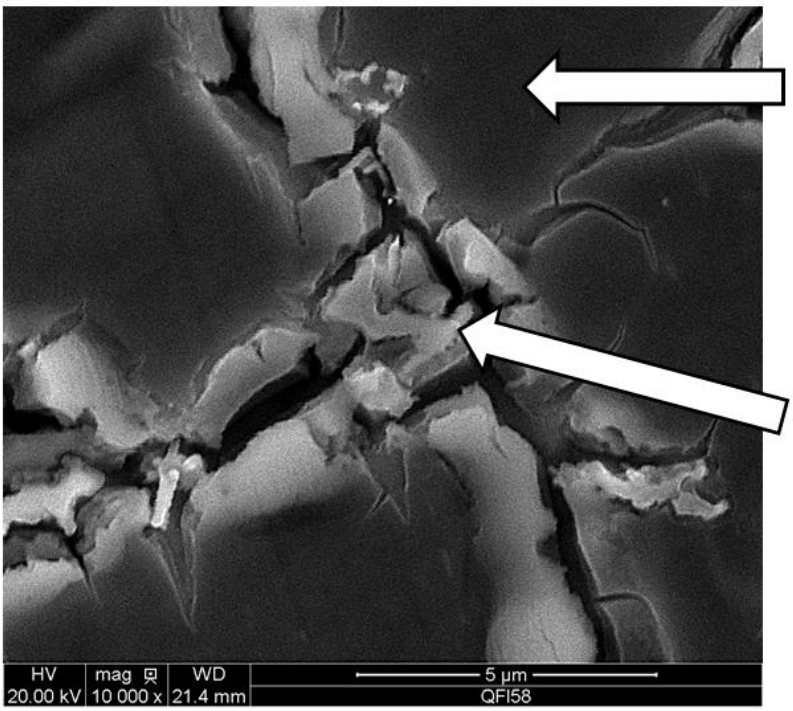

Element	wt.%
Ni	74.07±5
Cr	19.86±2
Nb	2.73±1
Mn	2.2±1
C	1.14±1

Element	wt.%
Ni	36.11±3
Cr	16.76±1
Nb	22.84±2
C	13.88±2
O	10.41±2

Figure 8. Composition in the intergranular and transgranular regions at a corrosion site of Inconel 600 after the DL-EPR test.

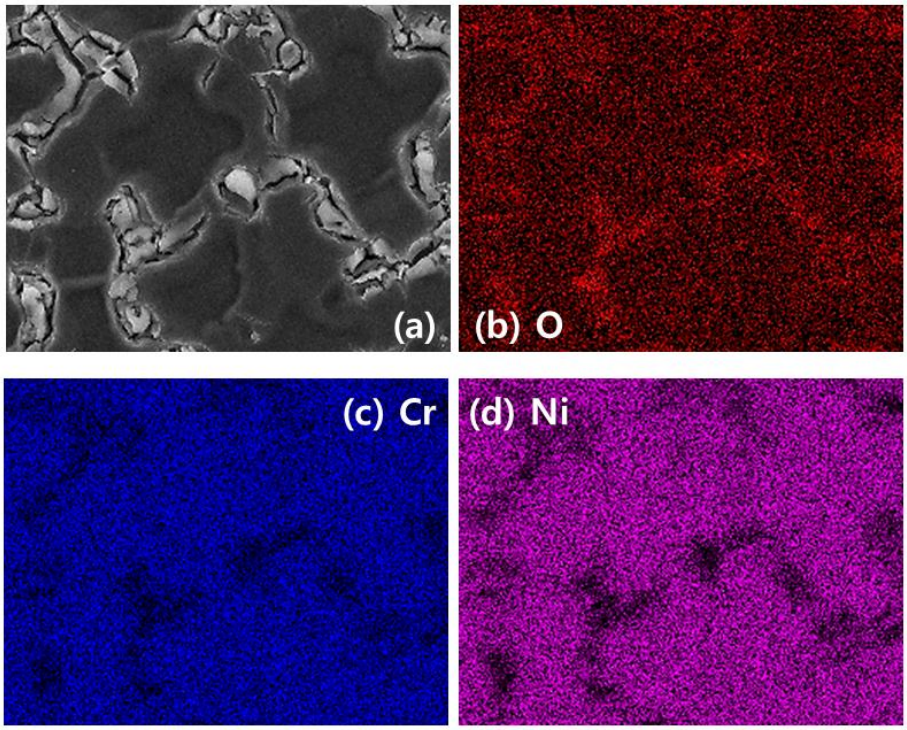

Figure 9. SEM–EDS images of analyzed composition mapping of the intergranular corrosion region in Inconel 600: (a) SEM image of intergranular corrosion region; mapping images of (b) oxygen, (c) chromium, and (d) nickel.

4. CONCLUSION

Based on the results of the potentiodynamic polarization tests, potentiostatic polarization tests, and DL-EPR tests to evaluate the electrochemical properties of Inconel 600 and Inconel 625 samples overlay-welded on A333 Grade 6 carbon steel, the following conclusion was obtained:

1. The potentiodynamic polarization tests showed that a relatively stable passive film was formed on both samples. When the two samples were compared, Inconel 625 had a higher corrosion potential (E_{corr}) and pitting potential (E_{pit}) than Inconel 600. In addition, Inconel 625 formed a marginally larger passive region (ΔE) than Inconel 600.

2. The potentiostatic polarization tests for observation of intergranular corrosion showed not much difference between the two samples. When the test was carried out at a potential of 1 V, which is below the pitting potential, the residual current of Inconel 625 was smaller and the stabilization rate was slightly faster. On the other hand, a larger difference was shown in the test conducted at a potential of 1.5 V, which is higher than the pitting potential.

3. Observation of the degree of sensitization (DOS) through the DL-EPR tests showed that the I_r/I_a value of DOS was about 0.01 for Inconel 600, which is within the fine sensitivity range. However, it was difficult to obtain the DOS of Inconel 625 because its I_r value did not appear on the graph of results. Observation of the surfaces after the corrosion test through SEM–EDS showed that a Cr-deficient region was formed on Inconel 600.

ACKNOWLEDGEMENTS
This investigation was supported by the Dong-A University Research Fund and the National Research Foundation of Korea (NRF) grant funded by Korea government (MEST) (No.NRF-2014R1A2A2A01002776).

References

1. J. C. Lippold, S. D. Kiser and J. N. DuPont, *Welding Metallurgy and Weldability of Nickel-Base Alloys*, John Wiley & Sons Inc., Hoboken, New Jersey, USA (2011) pp. 1–248.
2. O. H. Madsen, New technologies for waste to energy plants, in: *Proceedings of 4th International Symposium on Waste Treatment Technologies*, Sheffield, United Kingdom (2003).
3. Y.-H. Lee and I.-S. Kim: *Wear*, 253 (2002) 438.
4. F. T. Eberle, Dissimilar metal welded joint with protective overlay, U.S. Patent No. 2,963,129, 6 December 1960.
5. W. Woo, V. Em, C. R. Hubbard, H.-J. Lee, K. S. Park, *Mat. Sci. Eng. A*, , 528 (2011) 8021.
6. C.-C. Huang, R.-F. Liu, *Int. J. Pressure Vessels Piping*, 90 (2012) 77.
7. J. J. Kai, C. H. Tsai, T. A. Huang and M. N. Liu, *Metall. Mater. Trans. A*, 20 (1989) 1077.
8. K. H. Lee, G. Cragnolino and D. D. Macdonald, *Corrosion*, 41 (1985) 540.
9. G. P. Airey, *Corrosion,* 35 (1979) 129.
10. A. McMinn and R. A. Page: *Corrosion*, 44 (1988) 239.
11. T. Zaharinie, F. Yusof, M. Hamdi and T. Ariga, *Aust. J. Basic Appl. Sci.*, 8(19) (2014) -323.
12. E. Lunarska and Z. Szklarska-Smialowska, Hydrogen assisted fracture of Inconel 600 charged at high temperature, in: *Proceedings of International Congress on Fracture ICF7*, Houston, Texas, USA (2013).

13. I. B. Singh, *Corrosion*, 57, (2001) 483.
14. T. Baldridge, G. Poling, E. Foroozmehr, R. Kovacevic, T. Metz, V. Kadekar and M. C. Gupta, *Opt. Laser Eng.*, 51 (2013) 180.
15. H. X. Hu, Y. G. Zheng and C. P. Qin, *Nucl. Eng. Des.*, 240 (2010) 2721.
16. E. M. Lehockey, G. Palumbo and P. Lin, *Metall. Mater. Trans. A*, 29 (1998) 3069.
17. X. Xing, X. Di and B. Wang, *J. Alloy Compd.*, 593 (2014) 110.
18. M. J. Cieslak, T. J. Headley, A. D. Romig and T. Kollie, *Metall. Mater. Trans. A*, 19 (1988) 2319.
19. J. N. DuPont, *Metall. Mater. Trans. A*, 27 (1996) 3612.
20. L. Tan, X. Ren, K. Sridharan and T. R. Allen, *Corros. Sci.*, 50 (2008) 3056.
21. D. W. Kang and H. W. Lee, *Int. J. Electrochem. Sci.*, 9 (2014) 5864.
22. Corrosion of metals and alloys – Electrochemical potentiokinetic reactivation measurement using the double loop method (based on Cihal's method), *International Standard, ISO 12732*, International Organization for Standardization, Geneva, Switzerland (2008).
23. L. Y. Xu, M. Li, H. Y. Jing and Y. D. Han, *Int. J. Electrochem. Sci.*, 8 (2013) 2069.
24. J. R. Hayes, J. J. Gray, A. W. Szmodis and C. A. Orme, *Corrosion*, 62 (2006) 491.
25. J. L. Grosseau-Poussard, J. F. Dinhut, J. F. Silvain and R. Sabot, *Appl. Surf. Sci.*, 151 (1999) 49.
26. R. M. Deacon, J. N. DuPont and A.R. Marder, *Mat. Sci. Eng. A*, 460 (2007) 392.
27. X. Ren, K. Sridharan and T. R. Allen, *Corrosion*, 63 (2007) 603.
28. T. E. Abioye, D. G. McCartney and A. T. Clare, *J. Mater. Process. Technol.*, 217 (2015) 232.